Crystal Structure of Penicillin Binding Protein 4 (dacB) from *Escherichia coli*, both in the Native Form and Covalently Linked to Various Antibiotics†

Hiroyuki Kishida,‡ Satoru Unzai,‡ David I. Roper,§ Adrian Lloyd,§ Sam-Yong Park,*,‡ and Jeremy R. H. Tame*,‡

Protein Design Laboratory, Yokohama City University, Suehiro 1-7-29, Tsurumi-ku, Yokohama 230-0045, Japan, and Department of Biological Sciences, University of Warwick, Gibbet Hill Road, Coventry CV47AL, U.K.

Received August 1, 2005; Revised Manuscript Received November 15, 2005

ABSTRACT: The crystal structure of penicillin binding protein 4 (PBP4) from *Escherichia coli*, which has both DD-endopeptidase and DD-carboxypeptidase activity, is presented. PBP4 is one of 12 penicillin binding proteins in *E. coli* involved in the synthesis and maintenance of the cell wall. The model contains a penicillin binding domain similar to known structures, but includes a large insertion which folds into domains with unique folds. The structures of the protein covalently attached to five different antibiotics presented here show the active site residues are unmoved compared to the apoprotein, but nearby surface loops and helices are displaced in some cases. The altered geometry of conserved active site residues compared with those of other PBPs suggests a possible cause for the slow deacylation rate of PBP4.

The bacterial cell wall is a single molecule of peptidoglycan, which is essential for cell growth and survival under normal conditions. Since the enzymes involved in peptidoglycan synthesis have no counterpart in mammalian biochemistry, they present a variety of attractive and validated targets for antibiotic design. Many natural bacteriocidal compounds, including members of the penicillin family, also exploit the dependence of bacterial survival on the integrity of the cell wall. Penicillin derivatives remain an important class of antibiotics, but the growing problem of antibiotic resistance has led to renewed efforts to find new classes of antibacterials. Despite a great deal of research, the biological role of the various penicillin binding proteins (PBPs)[1] found in the periplasmic space of Gram-negative bacteria such as *Escherichia coli* remains poorly understood (*1*−*5*). Together, these proteins are responsible for peptidoglycan synthesis, repair, and hydrolysis, maintaining a stable cell wall while allowing the bacteria to grow. PBPs are the target of the β-lactam family of antibiotics which include penicillin and its derivatives. The inhibitory action of these drugs is based upon their structural similarity to the D-alanyl-D-alanine moiety present on peptidoglycan precursors (*6*). β-Lactams acylate the active site serine residue, blocking further catalytic activity.

Twelve PBPs have been characterized in *E. coli* (*1*). These are divided into two groups, with high and low molecular weight (MW). The high-MW PBP1a, PBP1b, PBP2, and PBP3 are bifunctional enzymes with both DD-transpeptidase and transglycosidase activities. Seven low-MW PBPs are known in *E. coli*, but none is essential (*1*). It has been concluded, on the basis of peptidoglycan composition on overexpressing PBP4, that the enzyme has both DD-endopeptidase and DD-carboxypeptidase activities (*7*), and was once suggested to be the endopeptidase responsible for breaking cross-links to insert new glycan chains (*8*). PBP4 from *E. coli* (encoded by dacB) is not directly related to PBP4s from Gram-positive bacteria, which are functionally equivalent to *E. coli* PBP5. Surprisingly, *E. coli* missing the genes for all the low-MW PBPs can survive and grow in rich medium, but together with PBP2 and PBP3, at least either PBP1a or PBP1b is essential, since they have the transpeptidase activity required to make peptidoglycan (*1*). PBP2 controls cell shape (without it, the cells become spheres instead of rods), and PBP3 is involved in septation. The remaining PBPs appear to play more specific roles; PBP5 is membrane-anchored and presumably acts to trim peptidoglycan close to the surface of the inner membrane. PBP4 is unusually sensitive to benzyl penicillin and ampicillin, which suggests an active site slightly different from those of other PBPs (*9*, *10*).

The low-MW PBPs are grouped into three classes (A, B, and C) by sequence (*11*, *12*). PBP4, a class C PBP, shows three short sequence motifs widely found in PBPs and β-lactamases, and it was suggested that PBP4 has a common ancestor with class A β-lactamases, but has acquired an extra domain of 188 residues (*13*). PBP5 from *E. coli* and *Streptomyces* R61 are well-studied members of classes A and B, respectively (*14*−*17*), but until recently, no crystallographic model of a class C PBP had been determined. Recently, the structure of a DD-peptidase/PBP from *Actinomadura* R39 which is similar to PBP4 has been published (*18*), the first model of its class. Although a crystallization report appeared 10 years ago (*19*), the structure of PBP4 from *E. coli* has not been published. We present high-resolution structures of PBP4, both in the absence of substrate

† S.-Y.P. is supported by the ISS applied research partnership program. J.R.H.T. also thanks the Japanese Society for the Promotion of Science for financial support.

* To whom correspondence should be addressed. E-mail: jtame@tsurumi.yokohama-cu.ac.jp and park@tsurumi.yokohama-cu.ac.jp. Telephone: +81 (0)45 508 7228. Fax: +81 (0)45 508 7366.

‡ Yokohama City University.

§ University of Warwick.

[1] Abbreviations: PBP, penicillin binding protein; IPTG, isopropyl β-D-thiogalactopyranoside; SeMet, selenomethionine.

10.1021/bi051533t CCC: $33.50
Published on Web 12/21/2005

Table 1: Data Collection and Refinement Statistics

	native	ampicillin	penicillin G	penicillin V	Farom	Flomox
refinement resolution (Å)	50.0−1.55	50.0−1.60	50.0−1.60	50.0−1.65	50.0−1.70	50.0−1.75
no. of reflections (measured/unique)	473198/75038	459562/68074	361461/68046	338643/61661	470700/58679	366163/52964
completeness[a] (%) (overall/outer shell)	95.9/77.8	95.2/69.9	94.6/76.3	94.4/72.1	98.4/89.0	96.9/78.7
R_{merge}[a,b] (%) (overall/outer shell)	5.4/36.4	6.0/31.1	7.7/36.1	5.7/40.4	5.4/34.4	5.3/33.0
redundancy (overall)	6.3	6.8	5.3	5.5	8.0	6.9
mean $\langle I/\sigma(I)\rangle$ (overall)	15.3	14.9	19.1	17.8	16.5	16.3
σ cutoff	0.0	0.0	0.0	0.0	0.0	0.0
R_{cryst}[c]/R_{free}[d] (%)	20.5/23.9	21.6/25.2	20.2/22.9	20.6/24.2	19.8/22.1	20.8/26.2
rmsd for bond lengths (Å)	0.014	0.015	0.013	0.015	0.015	0.017
rmsd for bond angles (deg)	1.4	1.4	1.4	1.5	1.5	1.6
no. of water atoms	349	268	303	229	251	168
average *B*-factor (Å^2) (protein/water/ligand)	30/37/*	32/37/28	31/36/28	31/38/30	29/36/42	35/38/63
Ramachandran plot						
residues in most favorable regions (%)	93.9	92.1	93.4	93.1	92.9	92.9
residues in additional allowed regions (%)	6.1	7.9	6.6	6.9	6.9	7.1

[a] Overall values and values for the highest-resolution shell (overall and outer shell, respectively). The highest-resolution shells from left to right are 1.81−1.75, 1.76−1.70, 1.71−1.65, 1.66−1.60, and 1.61−1.55 Å, respectively. [b] $R_{merge} = \sum|I_i - \langle I\rangle|/\sum|I_i|$, where I_i is the intensity of an observation and $\langle I\rangle$ is the mean value for that reflection. The summations are over all reflections. [c] $R_{cryst} = \sum_h||F_o(h)| - |F_c(h)||/\sum_h F_o(h)$, where F_o and F_c are the observed and calculated structure factor amplitudes, respectively. [d] R_{free} was calculated with 5% of the data excluded from the refinement.

and covalently linked to five different antibiotics, and compare it to other PBP structures.

EXPERIMENTAL PROCEDURES

The coding region for mature PBP4 (dacB) of *E. coli* was cloned from genomic DNA by PCR using the primers TTTGTGTCATATGGCAAATGTTGATGAGTACATTACTC and TTTGTGGGATCCTTAATTGTTCTGATAAATATCTTTATACAAACGGC. The product was then digested with NdeI and BamH1 and ligated into suitably cut pET21b. Sequencing a number of independent clones from separate PCR mixtures confirmed there is a single base change compared to the sequence expected from the genome sequence of *E. coli* K12, giving an Asp → Tyr mutation at position 261. Native and selenomethionine-containing protein were expressed by standard protocols. The plasmid was introduced into *E. coli* BL21(DE3) cells, which were grown to an optical density of 0.5 (600 nm) in LB medium at 20 °C. Expression was induced by adding IPTG to a final concentration of 0.2 mM, and growing the cells for a further 8 h. Cells were lysed by sonication in 50 mM Tris-HCl (pH 8.5) containing 30 mM NaCl and 15 mg/mL lysozyme. The lysate was centrifuged and applied to a Q-Sepharose column in 50 mM Tris-HCl (pH 8.5) and eluted with a salt gradient up to 300 mM NaCl. The protein was then dialyzed into 10 mM potassium phosphate (pH 6.8) and 300 mM NaCl and loaded onto a hydroxyapatite column (30 mL bed volume). The protein was eluted with 500 mM potassium phosphate and 500 mM NaCl. Following concentration, the protein was gel filtered using a HiLoad 16/60 Superdex 200 column washed with 20 mM MES (pH 6.5). The final protein was then concentrated to 10 mg/mL for crystallization (15 mg/mL for the SeMet derivative protein).

Crystals were obtained by the hanging drop method using a mother liquor of 0.1 M MES (pH 6.5) and 3−10% PEG 20000. Crystals were grown at 20 °C. Microseeding was necessary to produce single crystals of adequate size for analysis, and produced well-ordered crystals up to 0.7 mm long. Data collection and refinement statistics are given in Table 1. Prior to data collection, crystals were transferred to a cryoprotectant solution consisting of the same reservoir solution containing 25% (v/v) glycerol and were flash-cooled in liquid nitrogen. The crystals are in space group $P4_12_12$, and contain one molecule in the asymmetric unit. Crystals of antibiotic complexes were prepared by soaking native crystals for 2 h with mother liquid saturated with the relevant compound. Crystal soaking experiments using ampicillin, D-Ala-D-Ala, and D-Ala were carried out using 100 mM substrate for 24 h. Diffraction data were collected at PF BL5 and NW12A station, PF, Tsukuba, Japan, using an ADSC Quantum 315 CCD detector. The structure of PBP4 was initially determined to 2.5 Å resolution by the single-wavelength anomalous dispersion (SAD) method. Diffraction data were integrated and scaled with HKL2000 and SCALEPACK (*20*). General handling of the scaled data was carried out with programs from the CCP4 suite (*21*). The positions of Se atoms were determined using SOLVE, and density modification was carried out with RESOLVE (*22*, *23*). The resulting electron density map was sufficiently clear to build an initial model of the structure. The model was built with TURBO-FRODO (*24*). Structural refinement was performed using X-PLOR version 3.851 (*25*) and REFMAC (*26*). Solvent molecules were placed at positions where spherical electron density peaks were found above 1.3σ in the $2F_o - F_c$ map and above 3.0σ in the $F_o - F_c$ map and where stereochemically reasonable hydrogen bonds were allowed. Structural evaluations of the final models using PROCHECK (*27*) indicated that 90−93% of the residues are in the most favorable regions of the Ramachandran plot, with no residues in disallowed regions. A summary of the data collection and refinement statistics is given in Table 1. The models have been deposited with the Protein Data Bank as entries 2EX2 (native), 2EX6 (ampicillin bound), 2EX8 (penicillin G bound), 2EX9 (penicillin V bound), 2EXA (Farom bound), and 2EXB (Flomox bound).

RESULTS AND DISCUSSION

Cloning and Crystallization. The dacB gene of *E. coli* was cloned by PCR, omitting the 5′ region encoding the leader peptide which directs protein to the periplasm. The coding region for the mature protein (from residue 21) was inserted into the pET21 vector for high-level expression in the cytoplasm, permitting more than 5 mg of pure protein to be obtained from each liter of culture. Difficulties in expression

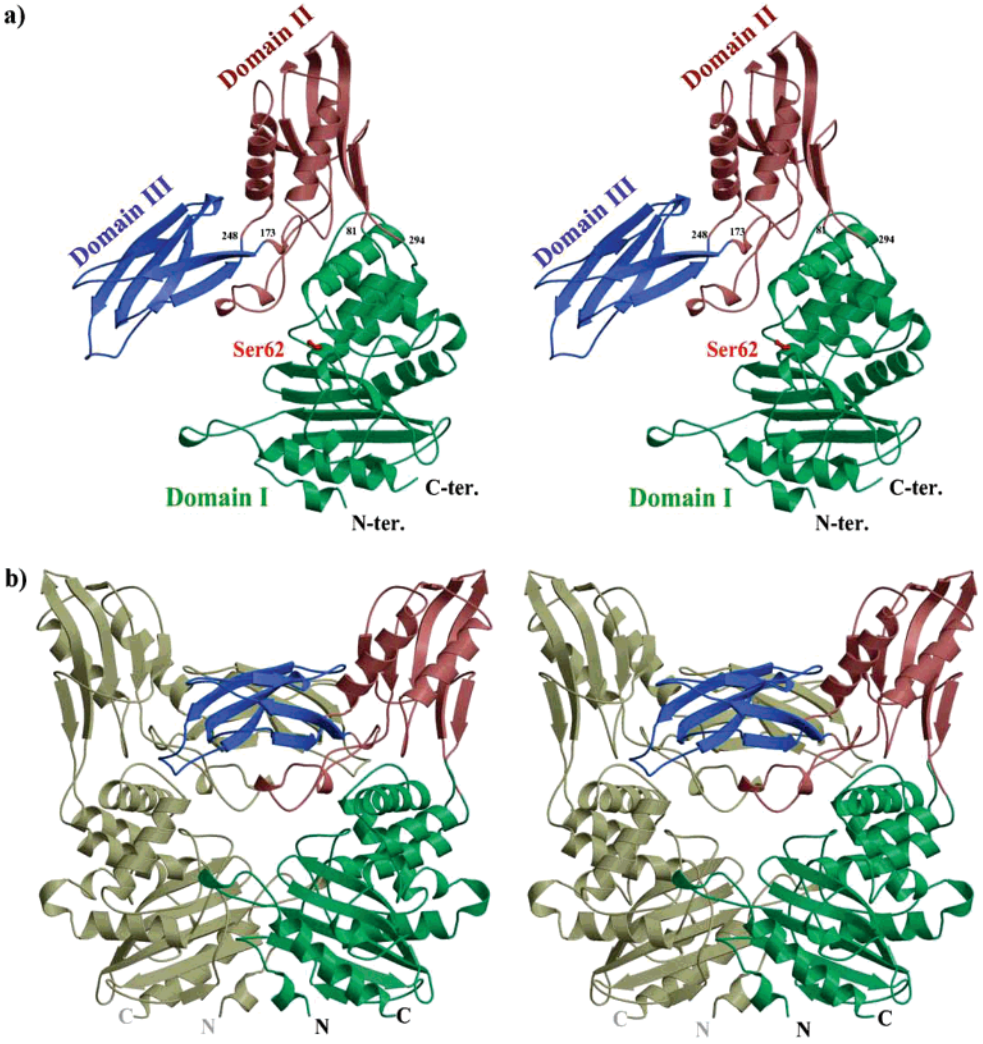

FIGURE 1: Overall structure of PBP4. (a) Ribbon diagram of the monomer, showing domains I, II, and III colored green, brown, and blue, respectively. α-Helices are shown as ribbons and β-strands as arrows. Domain I consists of residues 1−80 and 294−477, domain II residues 81−172 and 248−292, and domain III residues 173−247. Domain numbering was chosen for consistency with the convention chosen for R39 (*18*). The active site seine (Ser 62) is colored red. (b) Dimer present in solution, one partner being colored olive and the other colored as in panel a.

appear to have been the major stumbling block in previous attempts to determine the crystal structure; the protein was expressed with an N-terminal His tag, which led to protein aggregation in solution (*19*, *28*). We used the strategy of expressing only the globular part of the protein, which has been used before to enhance the yield of periplasmic proteins in the mature, soluble form (*29*). Crystals were obtained by routine screening and after optimization yielded X-ray diffraction to a resolution of 1.6 Å. Analytical ultracentrifugation analysis (sedimentation and equilibrium) showed the protein forms a tightly bound dimer (data not shown). The crystals are in space group $P4_12_12$, with a monomer in the asymmetric unit. Since there is only one crystallographic 2-fold symmetry axis, this must be the symmetry of the dimer in solution. A total surface area of 2320 Å^2 per monomer is buried at the dimer interface, consistent with a tightly bound dimer.

Overall Structure. The overall structure of the 457-residue protein shows three distinct domains, as shown in Figure 1, with domain III embedded in domain II, itself embedded in domain I. Throughout this paper, residue numbers refer to the full-length protein, although the crystals were grown from the globular portion beginning with Ala 21. The monomer has approximate dimensions of 80 Å × 65 Å × 30 Å. From one perspective, the Cα trace of the monomer shows a passing resemblance to the British Isles, with Ireland forming a separate domain III. This region, from Cys 173 to Ala 247, is formed from β-strands connected by short loops. Cys 173 forms a disulfide bond with Cys 159. The Cα atoms of Cys 173 and Ala 247 lie only 4.6 Å apart, and domain III has few contacts with the rest of the monomer so that it could probably be removed without unduly destabilizing the remainder of the structure. Despite its small size, this domain has a well-ordered hydrophobic core, suggesting it could form a stable globular protein on its own. It contributes roughly 1000 Å^2 (40%) of the dimer interface area (Figure 1b). The two copies of domain III within the dimer contact each other only through Asp 205, which hydrogen bonds to its symmetry mate.

The bulk of the structure is built from domain I and domain II, each having an antiparallel five-stranded β-sheet and associated α-helices, the chain passing twice between the sheets, and the C-terminus ending close to the N-terminus in domain I. It has been suggested on the basis of sequence

alignments that PBP4 is evolutionarily related to β-lactamases, but carries an insertion of 188 residues shortly after the active site serine, Ser 62 (*13*). The crystal structure supports this idea but shows the insertion is slightly longer, and consists of the 218 residues making up domains II and III. Sequence comparison with the Protein Data Bank shows PBP4 closely matches only one entry, 1D2F, a pyridoxal phosphate-dependent enzyme with no known relation to PBPs (*30*). The two sequences are almost 11% identical overall, but with no region of special similarity. Searching the Protein Data Bank with DALI (*21*) yielded no known protein structures similar to PBP4 or domain III. Additional searches with SSM (*31*) also failed to find a close match to the protein. Unusual features of the protein include the edge strand of β-sheet 2 from Ser 271 to Arg 276. The chain continues by crossing the β-sheet, and residues Ala 288 to Ser 292 form the opposite edge of the same β-sheet, with the same orientation as the previous strand.

While this paper was being prepared, a report of the structure of DD-peptidase from Gram-positive *Actinomadura* sp. R39 appeared (*18*). This protein ("R39") exhibits a structure very similar to that of PBP4, but is monomeric. The 400 C-terminal residues of the two proteins are 28% identical, but R39 has a signal sequence rather longer, 49 residues, than the 21-residue leader peptide on PBP4. A sequence alignment of PBP4 with R39 and two other PBPs is shown in Figure 2. R39 is significantly more similar (45% identical over 453 residues) to a putative PBP from *Bacillus subtilis*. Overall, the structures of PBP4 and R39 are very similar, the main differences being found in loop regions, especially just before the final helix in the loop from Tyr 448 to Pro 461 in PBP4. The regions with the highest degree of conservation with PBP4 closely match the active site, but also include the sequence DPTL (from Asp 95 in R39 and Asp 108 in PBP4) which forms a turn. Sauvage and colleagues have suggested that domain II of R39 may serve to bind other components of the septation machinery (*18*), but no patch of conserved surface residues indicates an obvious binding site. They also implicate Trp 139 in peptidoglycan binding by R39, a function which may be served by Trp 153 in PBP4. Domain III also shows differences between the two proteins, PBP4 notably including a short insertion from Ser 211 to Cys 217 relative to R39. Cys 217 forms a disulfide bond with Cys 234 to stabilize this extra loop, which lies close to Phe 323 and Thr 325 in the partner chain. Tyr 216 and Glu 218 form hydrogen bonds with Asp 334 and Arg 330, respectively, in the partner protein.

Active Site. The active site serine is found at the bottom of an open groove on the protein surface, readily accessible to small molecules such as ampicillin. β-Sheet 1 and domain III lie on either side of the active site, creating a U-shaped valley roughly 20 Å deep and 15 Å across (Figure 3). Long thin substrates appear to be able to reach the active site more easily than bulky ones, and one function of domain III may be steric control of substrate access. R39 rapidly hydrolyzes small synthetic substrates, demonstrating these can readily enter the active site (*32*). The active site of PBP4 is formed by an edge strand of β-sheet 1 (Gly 419−Leu 421), a turn between two helices (Lys 305−Asn 308), and a section of coil (Asn 154−Ser 161). The active site serine (Ser 62) is found at the start of helix 1. This region is well-ordered in the electron density map even in the absence of substrate. Ala 61 has unusual ϕ and ψ angles, 52° and 141°, respectively, despite the remainder of the structure showing no unexpected features in the Ramachandran plot. The distance between the carbonyl oxygens of Ala 61 and Pro 60 is only 3.0(6) Å.

Comparison with much-studied related enzymes shows PBP4 to have all the groups necessary to activate the serine hydroxyl for nucleophilic attack, including the "SXXK", "SXN", and "KTG" motifs characteristic of PBPs. The SXXK motif includes the active site serine, and the lysine (Lys 65 in PBP4 and Lys 52 in R39) clearly plays an important role in organizing the nearby residues as well as reducing the pK_a of the serine hydroxyl group. Overlapping the structures of PBP4 and R39, one can see the active sites are highly similar with Lys 417, Thr 418, and Ser 306 sitting in locations identical to those of their counterparts in R39. These residues form a hydrogen bond network with Ser 62 and Lys 65. The lysine and threonine form the highly conserved KTG motif, and Ser 306 starts the SXN motif. In apo-PBP4, Asn 308 forms a hydrogen bond with Lys 65 [2.6-(5) Å long] through its side chain oxygen. The importance of the conserved Asn has been demonstrated with several PBPs (*14*, *33*). The precise mechanism of acylation of the active site serine is uncertain, and may involve separate nucleophilic attack and return of a proton to the substrate, or a concerted mechanism. In either case, Lys 65 abstracts a proton from the hydroxyl group of Ser 62, and Ser 306 returns a proton to the nitrogen in the β-lactam ring.

Structures of Covalent Adducts. To observe the interactions between PBP4 and different penicillin derivatives, crystals of apo-PBP4 were soaked with five different compounds. In these structures, Ser 62 is covalently linked to the substrate via an ester linkage. With the exception of Flomox (cefapeme pivoxil hydrochloride), these all yielded very clear electron density into which the antibiotics could be readily modeled. Electron density maps for these adducts are shown in Figure 4. In the case of the ampicillin complex, Ser 420 makes two hydrogen bonds to the adduct, through its N atom to the ester carbonyl and through its carbonyl to the ampicillin amide nitrogen. Asn 308 hydrogen bonds to the ampicillin amide oxygen. The benzene ring of the antibiotic contacts Phe 160 in an edge-to-face fashion. Lys 65 makes several hydrogen bonds, with the side chains of Ser 62, Asn 308, and Ser 306, the latter also hydrogen bonding to the nitrogen of the ampicillin 5mer ring. Overlaying the structure of the protein with and without substrate shows no significant movements in the active site.

Although the active site shows very little movement on binding, small shifts are found near the N- and C-termini in some of the complexes. For example, Flomox places a methyl ester group very close to the position of Leu 421 in the apo crystal structure. A short hairpin loop from Ser 420 to Tyr 425 is pushed away from the active site, the Cα atom of Gln 422 moving ~3 Å. The loop in turn presses against the last strand of the first β-sheet in domain 1 (residues 438−448), disordering the loop from Ala 449 to Arg 459, and moving the N- and C-terminal α-helices between 2 and 4 Å along their axes. The penicillin V and penicillin G adducts do not exhibit these movements, but residues 452−459 and the six N-terminal residues do become disordered with penicillin V in the binding site. Ampicillin also disorders

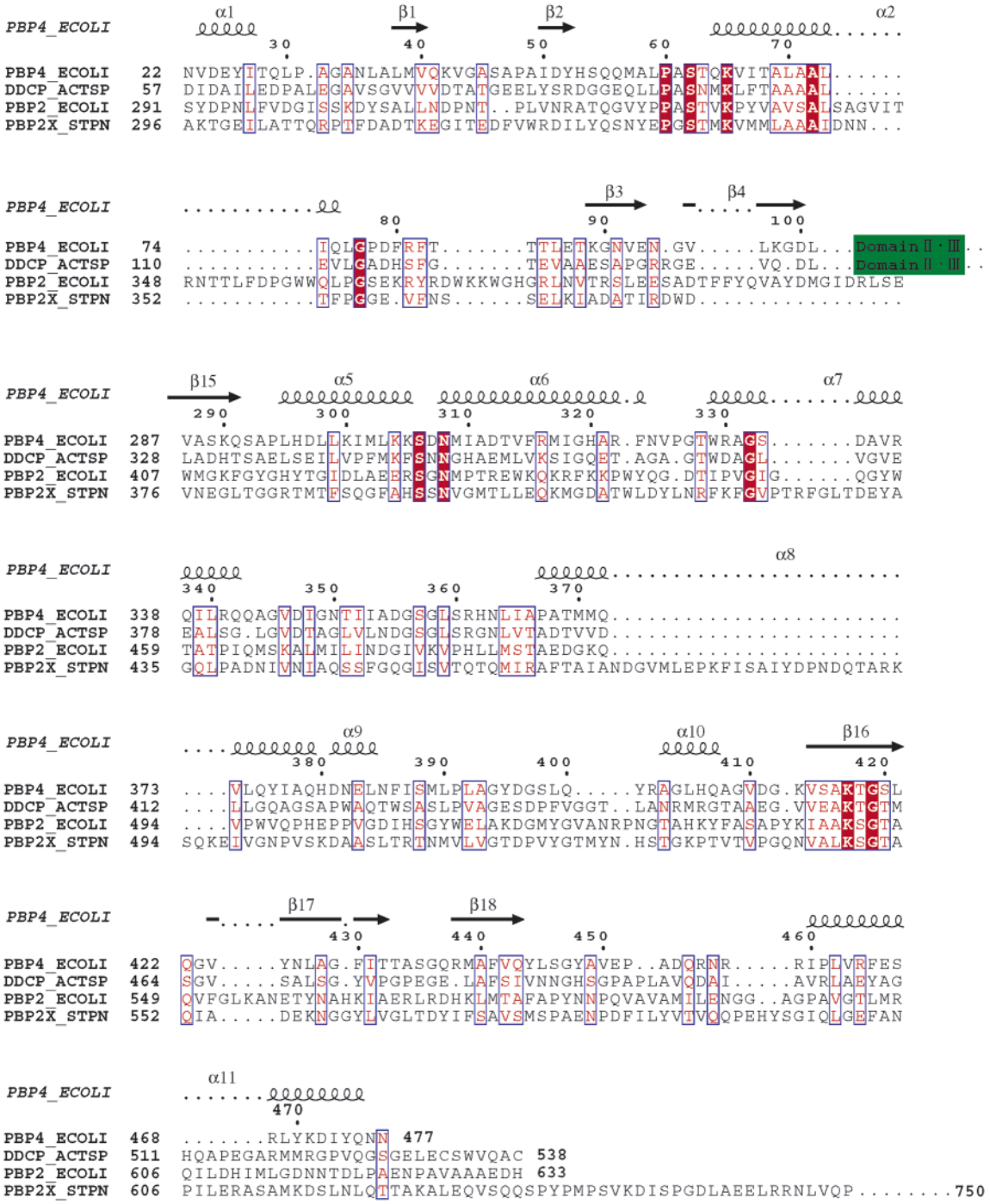

FIGURE 2: Sequence alignment of domain I of PBP4 with R39 ("DDCP_ACTSP", SwissProt entry P39045), *E. coli* PBP2 (SwissProt entry P08150), and *Streptococcus pneumoniae* PBP2x (SwissProt entry P14677). Note that the PBP4 models described here have a single mutation, D261Y, relative to the SwissProt entry (P24228), on the protein surface roughly 35 Å from the active site. Secondary structure is indicated with arrows and coils for β-strands and α-helices, respectively. Residues common to all four sequences are depicted with white letters on a red background. These residues closely match the active site motifs beginning with Ser 62, Ser 306, and Lys 417. Domains II and III do not contribute to the active site.

the N-terminal helix without disturbing residues 449−459. None of the motions on substrate binding appears to be able to support cooperativity between the two active sites of the dimer, which are nearly 28 Å apart, and it seems highly likely that the subunits function independently. The rms deviations for the main chain atoms of the different complexes compared to apo-PBP4 are given in Table 2.

The second part of the reaction cycle, the deacylation to free the serine from covalent attachment to the substrate, is less well understood than the acylation. Quantum mechanical methods have been used to analyze the different rates in PBPs and β-lactamases (*34*). Even with the very large body of research dedicated to PBP5, including kinetic analysis and crystal structures of the native protein and site-directed mutants, and an inhibitor complex structure, Nicola and colleagues conceded recently that a comprehensive understanding of the PBP5 catalytic mechanism has "proven elusive" (*35*). They further point out that the deacylation mechanism need not necessarily be the same for peptide substrates and β-lactam antibiotics, but appears to involve a

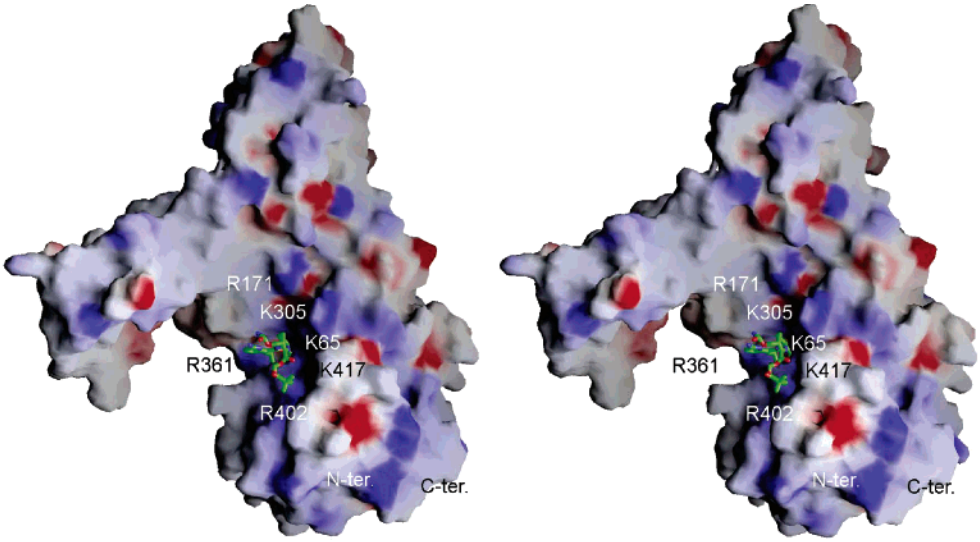

FIGURE 3: Molecular surface of the PBP4 monomer, colored by charge, showing the positive potential around the active site. Full color saturation (red for negative, blue for positive) corresponds to an electron energy of $\pm 20 k_B T$. Lysine and arginine residues in this region are indicated, including Lys 65 and Lys 417. Ampicillin in the active site is shown as a ball-and-stick model, showing the cleft between domains I and III easily accommodates small antibiotics. Domain III may prevent highly cross-linked peptidoglycan from reaching the active site.

subtle network of polarizing interactions. Far less research has so far been published on PBP4, which is unusually susceptible to penicillins. In testing the effectiveness of a new penicillin derivative, Farom (faropenem sodium), Ishiguro and colleagues found only PBP2 of *E. coli* is more readily inhibited (*36*). Some clues about the slow deacylation rate are found by comparing PBP4 with two class A structures, PBP5 from *E. coli* and TEM1 β-lactamase.

Comparison with TEM1. β-Lactamases are enzymes which have evolved to hydrolyze penicillins and cephalosporins, rendering the host bacteria immune to these antibiotics. Among the β-lactamases, class A TEM1 is one of the most studied; crystal structures are known of both mutants and inhibitor complexes (*33*, *37*), and electrostatic analysis has been carried out to analyze the catalytic efficiency (*38*). Comparing PBP4 with TEM1 shows that these enzymes do share topology, despite the failure of DALI and SSM to locate similar structures in the Protein Data Bank. In fact, PBP4 shows almost all the secondary structures of TEM1 except the first α-helix. Mature TEM1 is 262 residues long and corresponds to domain I in PBP4. Overlaying the two structures on only the four Cα atoms of the SXXK motif (Ser 62−Lys 65 in PBP4 and Ser 70−Lys 73 in TEM1) gives a remarkably good fit over the whole Cα trace of TEM1, though the loop regions are clearly less conserved and exhibit a number of small insertions. Residues 79 and 294 in PBP4 correspond to residues 92 and 118 in TEM1, respectively. Around the active site (Figure 5), the β-hairpin from Ser 415 to Phe 430 is also found in TEM1, and the active site serine is found at the same point at the start of helix 1 (helix 2 in TEM1). Ser 130−Asn 132 of TEM1 overlay closely on Ser 306−Asn 308 of PBP4 (the SXN motif), and Lys 234 matches Lys 417 of PBP4 (the KTG motif). There are, however, marked differences; the loop from Asp 355 to Leu 359 in PBP4 is not present in TEM1. Also, the Ω-loop in TEM1 (residues 161−180) has no counterpart in PBP4. This loop carries Glu 166, which is responsible for the deacylation reaction via activation of a nearby water molecule to attack nucleophilically the intermediate ester. Deacylation is the rate-limiting step of penicillin hydrolysis by TEM1, and replacing Glu 166 with tyrosine reduces the deacylation rate 4000-fold (*39*, *40*). Deacylation is much slower in PBP4, and clearly cannot proceed by the same mechanism. PBP4 has a serine, Ser 357, close to the active site which overlays with Glu 166 of TEM1. Asp 312 hydrogen bonds with the main chain nitrogen atoms of Gly 356 and Ser 357, and also to the γ-hydroxyl of the serine. This hydroxyl oxygen lies ~7.2 Å from the ester carbon atom, and a water molecule positioned halfway along the line between these two atoms would hydrogen bond to the side chain of Asn 308 and be in a favorable position for nucleophilic attack. PBP4 has no equivalent of Asn 170 in TEM1 which also hydrogen bonds to the nucleophilic water molecule. A small positive peak in the $F_o - F_c$ density map of the ampicillin complex suggests a water molecule may be very weakly held in a suitable position for attack on the acyl intermediate, but the occupancy is very low. The other complexes show no evidence of a water molecule in this position. The lack of a suitably positioned and activated water molecule provides the most convincing explanation for the reported slow deacylation step, which makes ampicillin a potent inhibitor of PBP4. Clearly, further work is required to test this hypothesis, however.

Comparison with PBP5. Like PBP4, PBP5 is a low-MW PBP which plays a role in maintaining cell morphology, but which shows a high deacylation rate. The crystal structure of a deacylation defective engineered mutant of PBP5 from *E. coli* was determined several years ago (*14*), and models of the apoprotein and inhibitor-bound wild-type protein have appeared since (*15*, *35*). PBP5 is membrane-anchored by an N-terminal hydrophobic leader sequence which was removed to prepare crystals of the globular domain. Comparing PBP5 (PDB entry 1NZO) with PBP4 again shows the two proteins share topology around the active site, but PBP5 has an extra C-terminal domain from residue 263 which has no counterpart in PBP4, and does not have domains II and III of PBP4. Thus, the active site of PBP5 is more exposed than that of PBP4, but PBP5 is restricted to the membrane in vivo, which

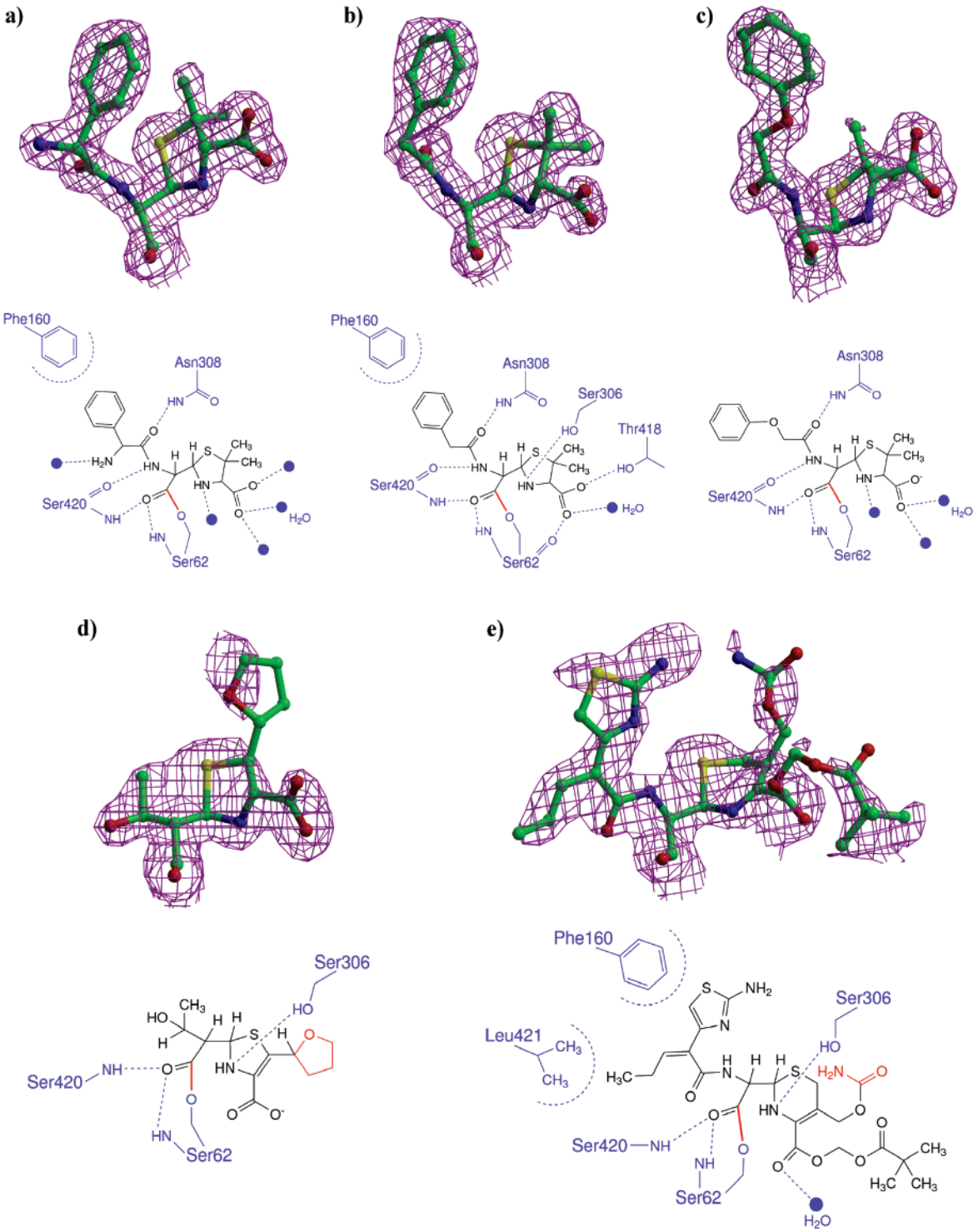

FIGURE 4: $2mF_o - DF_c$ electron density maps covering the antibiotic moiety covalently attached to Ser 62 of PBP4. The drug moieties are shown as ball-and-stick models with carbon atoms colored green, oxygens red, nitrogens blue, and sulfurs yellow. All maps are shown at the 1σ contour level, and beside each is a figure showing the unreacted antibiotic. Disordered parts of the molecule are colored red, as is the covalent link to the protein: (a) ampicillin, (b) penicillin G, (c) penicillin V, (d) Farom, and (e) Flomox. Hydrophobic groups such as the phenyl group on penicillin G and ampicillin lie close to Phe 160, and the ester carbonyl oxygen hydrogen bonds to the main chain nitrogen of Ser 420. Few other interactions are formed with the protein, except that Asn 308 hydrogen bonds to the amide carbonyl in the case of the two penicillin derivatives and ampicillin.

presumably prevents uncontrolled digestion of the peptidoglycan layer. Overlapping the Cα atoms of the SXXK motif of the two proteins (Ser 62−Lys 65 in PBP4 and Ser 44−Lys 47 in PBP5) shows the active sites retain many similar features (Figure 6). Lys 417 and Asn 308 of PBP4 overlap Lys 213 and Asn 112 of PBP5, and the two enzymes share a leucine residue (359 in PBP4 and 153 in PBP5) which is not found in TEM1. There are also clear differences between PBP4 and PBP5. In PBP4, the amine side chain of Lys 417 (of the KTG motif) hydrogen bonds to the side chain hydroxyl of Thr 418. In PBP5, the threonine adopts a different rotamer, and the lysine hydrogen bonds to Ser 110

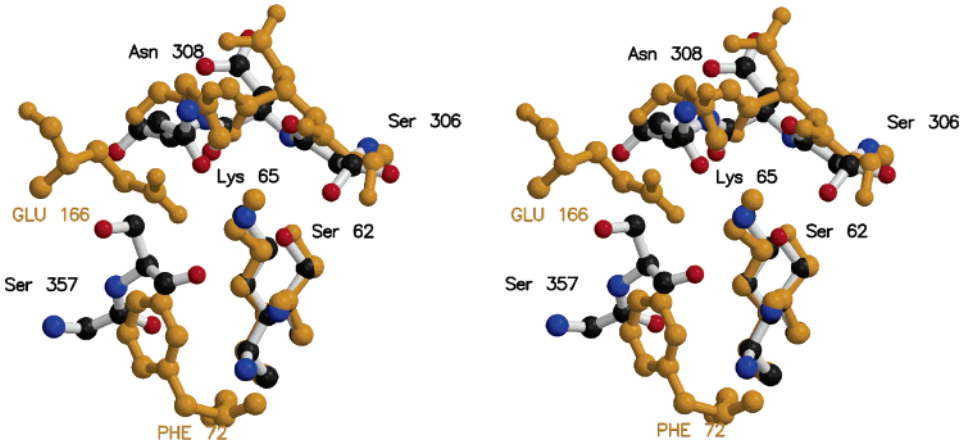

FIGURE 5: Stereo overlay of apo-PBP4 with TEM1 (PDB entry 1BTL), showing the main active site residues. The main chain atoms of Ser 62−Lys 65 (PBP4) were least-squares fitted to those of Ser 70−Lys 73 in TEM1. PBP4 residues are colored by atom type and labeled in black. TEM1 residues are colored and labeled in orange. The SXXK and SXN motifs match closely, and Ser 130 in TEM1 lies close to Ser 306 in PBP4 (only the major conformer of the Ser 306 side chain is shown for clarity). PBP4 has no counterpart to Glu 166 of TEM1, however, the closest residue being Leu 359. Together with Asn 170, Glu 166 makes the active site of TEM1 much more polar than that of PBP4. The carbonyl oxygen of Ser 357 in PBP4 points toward Ser 62, and lies ~3.7 Å from the active site serine side chain oxygen atom. The carboxyl side chain of Glu 166 in TEM1 lies slightly farther (~4.2 Å) from its active site serine. Figures 5−7 were produced with Molscript (*41*) and Raster3D (*42*).

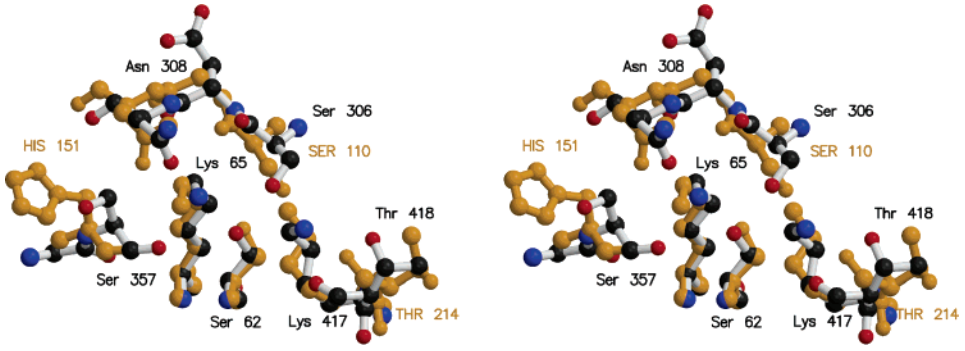

FIGURE 6: Stereo overlay of the active sites of PBP4 and PBP5 from *E. coli*. The main chain atoms of Ser 62−Lys 65 (PBP4) were least-squares fitted to those of Ser 44−Lys 47 in PBP5 (PDB entry 1NZO). PBP5 residues are colored and labeled in orange. The carbonyl oxygen atom of His 151 in PBP5 lies in a position and orientation similar to those of Ser 357 in PBP4, and was originally suggested to play a role in the enzyme mechanism. Attention has now centered on Ser 110, which adopts a conformation slightly different from that of Ser 306 in PBP4. The conformations of the KTG motif lysine (Lys 417 in PBP4 and Lys 213 in PBP5) are also different.

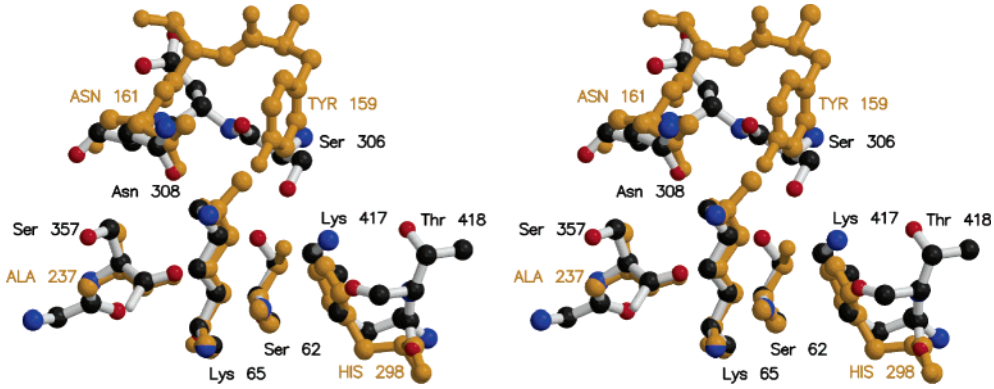

FIGURE 7: Stereo overlay of PBP4 and R61 (PDB entry 3PTE). The structures were fitted using the main chain atoms of Ser 62−Lys 65 in PBP4 and Ser 62−Lys 65 in R61. R61 residues are colored and labeled in orange. The active site of R61 is more different from PBP4 than TEM1 or PBP5. Lys 417 is replaced with a histidine and Ser 306 with a tyrosine (only the main conformer of Tyr 159 is shown for clarity). The carbonyl oxygen of Ser 357 in PBP4 closely fits the carbonyl of Ala 237 in R61.

of the SXN motif. The largest difference lies around Ser 357 and Asp 312 of PBP4. As described above, these replace Glu 166 of the Ω-loop found in TEM1, and probably explain the very different rates of deacylation in the two enzymes. The chain trace of PBP5 is different again, placing a histidine in this position (His 151). The histidine lies on the other side of Leu 153 from Ser 44 (the active serine of PBP5) so its role in deacylation is not clear. It has been suggested that the carbonyl oxygen of His 151 may promote deacylation by activating a water molecule (*14*). This oxygen atom lies 5.1 Å from the active site serine hydroxyl of PBP5, compared to 3.7 Å between the carbonyl oxygen of Ser 357 and the

Table 2: Root-Mean-Square Deviations between the Native Structure and the Other Complex PBPs[a]

	ampicillin	penicillin G	penicillin V	Farom	Flomox
rmsd (Å)	0.247	0.136	0.206	0.347	0.425

[a] The root-mean-square deviations of main chain atoms of residues 40−400 inclusive.

active site hydroxyl in PBP4. Water can possibly more easily access the acyl intermediate of PBP5 because of the more open active site; however, Glu 166 of TEM1 also sits within 4 Å of the active site serine, and the conserved active site residues of PBP4 more closely resemble TEM1 than those of PBP5. Disrupting the SXN motif dramatically slows the deacylation, and a recently determined crystal structure of PBP5 suggests that Lys 213 and Ser 110 of PBP5 are needed to activate the attacking water molecule (*15*, *35*). The slower deacylation rate of PBP4 may therefore be due to the notably different conformations of its residues in the SXN and KTG motifs. Serine is not absolutely required at the active site among PBPs since the class B enzyme R61 replaces the SXN motif serine with tyrosine (Figure 7). R61 notably retains Asn and Lys residues which overlap very closely with Asn 308 and Lys 417 of PBP4, respectively.

CONCLUSION

The high-resolution crystal structure of PBP4 (dacB) from *E. coli* shows the protein to be related to other PBPs and β-lactamases, as predicted from the presence of sequence motifs and sequence similarity. The active site appears to be little changed by the presence of ampicillin or other antibiotics covalently linked to the active site serine, and there is no evidence of cooperativity between the symmetry-related sites of the dimer. While the catalytic groups involved in nucleophilic attack on substrates are relatively well conserved, compared to PBP5 and TEM1, there are clear differences in the mechanism of deacylation. In the case of TEM1, this may reflect the need for the enzyme to turn over substrate as rapidly as possible to allow the host bacteria to survive in the presence of antibiotics. PBP4 and PBP5 are not essential, and it may be that a very high turnover rate is not required.

Since the antibiotic resistance marker of the expression vector that was used (pET21) is ampicillin resistance, ampicillin was added to the cultures on inoculation. Fresh antibiotic was not added upon addition of IPTG to induce expression of PBP4. The fact that no ampicillin is found in the active site of the purified protein suggests it is largely hydrolyzed before PBP4 overexpression, and PBP4 can remove any remaining ampicillin slowly over the course of purification. Soaking the crystals with ampicillin readily gives the covalent adduct. Soaks with D-Ala-D-Ala and D-Ala produced no changes in the electron density map to indicate binding, however, despite the open and seemingly rigid binding site. Isothermal titration calorimetry experiments also failed to give any indication that ampicillin, D-Ala-D-Ala, or D-Ala interacts with the protein (data not shown). This may be due to binding with a very small heat change, but the inability to observe the presumed natural substrate and product in the binding site by crystal soaking implies that additional interactions with the peptidoglycan are required for binding. The crystal structures presented here provide a useful starting point for further studies to examine the reaction mechanism. Studies are currently underway to examine the substrate preferences of PBP4 using various peptidoglycan fragments with specific compositions.

ACKNOWLEDGMENT

We thank Prof. S. Wakatsuki and Drs. N. Igarashi and N. Matsugaki of the Photon Factory for help with data collection.

REFERENCES

1. Denome, S. A., Elf, P. K., Henderson, T. A., Nelson, D. E., and Young, K. D. (1999) *Escherichia coli* mutants lacking all possible combinations of eight penicillin binding proteins: Viability, characteristics, and implications for peptidoglycan synthesis, *J. Bacteriol. 181*, 3981−93.
2. Meberg, B. M., Paulson, A. L., Priyadarshini, R., and Young, K. D. (2004) Endopeptidase penicillin-binding proteins 4 and 7 play auxiliary roles in determining uniform morphology of *Escherichia coli*, *J. Bacteriol. 186*, 8326−36.
3. Nelson, D. E., and Young, K. D. (2001) Contributions of PBP 5 and DD-carboxypeptidase penicillin binding proteins to maintenance of cell shape in *Escherichia coli*, *J. Bacteriol. 183*, 3055−64.
4. Popham, D. L., and Young, K. D. (2003) Role of penicillin-binding proteins in bacterial cell morphogenesis, *Curr. Opin. Microbiol. 6*, 594−9.
5. Young, K. D. (2003) Bacterial shape, *Mol. Microbiol. 49*, 571−80.
6. Tipper, D. J., and Strominger, J. L. (1965) Mechanism of action of penicillins: A proposal based on their structural similarity to acyl-D-alanyl-D-alanine, *Proc. Natl. Acad. Sci. U.S.A. 54*, 1133−41.
7. Korat, B., Mottl, H., and Keck, W. (1991) Penicillin-binding protein 4 of *Escherichia coli*: Molecular cloning of the dacB gene, controlled overexpression, and alterations in murein composition, *Mol. Microbiol. 5*, 675−84.
8. Burman, L. G., and Park, J. T. (1984) Molecular model for elongation of the murein sacculus of *Escherichia coli*, *Proc. Natl. Acad. Sci. U.S.A. 81*, 1844−8.
9. Matsuhashi, M., Takagaki, Y., Maruyama, I. N., Tamaki, S., Nishimura, Y., Suzuki, H., Ogino, U., and Hirota, Y. (1977) Mutants of *Escherichia coli* lacking in highly penicillin-sensitive D-alanine carboxypeptidase activity, *Proc. Natl. Acad. Sci. U.S.A. 74*, 2976−9.
10. Spratt, B. G., and Pardee, A. B. (1975) Penicillin-binding proteins and cell shape in *E. coli*, *Nature 254*, 516−7.
11. Ghuysen, J. M. (1991) Serine β-lactamases and penicillin-binding proteins, *Annu. Rev. Microbiol. 45*, 37−67.
12. Massova, I., and Mobashery, S. (1998) Kinship and diversification of bacterial penicillin-binding proteins and β-lactamases, *Antimicrob. Agents Chemother. 42*, 1−17.
13. Mottl, H., Nieland, P., de Kort, G., Wirenga, J. J., and Keck, W. (1992) Deletion of an additional domain located between SXXK and SXN active-site fingerprints in penicillin-binding protein 4 from *Escherichia coli*, *J. Bacteriol. 174*, 3261−9.
14. Davies, C., White, S. W., and Nicholas, R. A. (2001) Crystal structure of a deacylation-defective mutant of penicillin-binding protein 5 at 2.3-Å resolution, *J. Biol. Chem. 276*, 616−23.
15. Nicholas, R. A., Krings, S., Tomberg, J., Nicola, G., and Davies, C. (2003) Crystal structure of wild-type penicillin-binding protein 5 from *Escherichia coli*: Implications for deacylation of the acyl-enzyme complex, *J. Biol. Chem. 278*, 52826−33.
16. Silvaggi, N. R., Josephine, H. R., Kuzin, A. P., Nagarajan, R., Pratt, R. F., and Kelly, J. A. (2005) Crystal structures of complexes between the R61 DD-peptidase and peptidoglycan-mimetic β-lactams: A non-covalent complex with a "perfect penicillin", *J. Mol. Biol. 345*, 521−33.
17. Silvaggi, N. R., Kaur, K., Adediran, S. A., Pratt, R. F., and Kelly, J. A. (2004) Toward better antibiotics: Crystallographic studies of a novel class of DD-peptidase/β-lactamase inhibitors, *Biochemistry 43*, 7046−53.
18. Sauvage, E., Herman, R., Petrella, S., Duez, C., Bouillenne, F., Frere, J. M., and Charlier, P. (2005) Crystal structure of the

actinomadura R39 DD-peptidase reveals new domains in penicillin-binding proteins, *J. Biol. Chem. 29*, 29.
19. Thunnissen, M. M., Fusetti, F., de Boer, B., and Dijkstra, B. W. (1995) Purification, crystallisation and preliminary X-ray analysis of penicillin binding protein 4 from *Escherichia coli*, a protein related to class A β-lactamases, *J. Mol. Biol. 247*, 149−53.
20. Otwinowski, Z., and Minor, W. (1997) Processing of X-ray diffraction data collected in oscillation mode, *Methods Enzymol. 276*, 307−26.
21. Collaborative Computational Project No. 4 (1994) The CCP4 suite: Programs for protein crystallography, *Acta Crystallogr. D50*, 760−3.
22. Terwilliger, T. C. (2003) SOLVE and RESOLVE: Automated structure solution and density modification, *Methods Enzymol. 374*, 22−37.
23. Terwilliger, T. C., and Berendzen, J. (1999) Automated MAD and MIR structure solution, *Acta Crystallogr. D55*, 849−61.
24. Roussel, A., and Cambillau, C. (1989) in *Silicon Graphics Geometry Partners Directory*, pp 77−8, Silicon Graphics, Mountain View, CA.
25. Brunger, A. T. (1996) *X-PLOR*, version 3.851, Yale University Press, New Haven, CT.
26. Murshudov, G. N., Vagin, A. A., and Dodson, E. J. (1997) Refinement of macromolecular structures by the maximum-likelihood method, *Acta Crystallogr. D53*, 240−55.
27. Laskowski, R. A., MacArthur, M. W., Moss, D. S., and Thornton, J. M. (1993) PROCHECK: A program to check the stereochemical quality of protein structures, *J. Appl. Crystallogr. 26*, 283−91.
28. Fusetti, F., and Dijkstra, B. W. (1996) Purification and light-scattering analysis of penicillin-binding protein 4 from *Escherichia coli*, *Microb. Drug Resist. 2*, 73−6.
29. Heddle, J., Scott, D. J., Unzai, S., Park, S. Y., and Tame, J. R. (2003) Crystal structures of the liganded and unliganded nickel-binding protein NikA from *Escherichia coli*, *J. Biol. Chem. 278*, 50322−9.
30. Clausen, T., Schlegel, A., Peist, R., Schneider, E., Steegborn, C., Chang, Y. S., Haase, A., Bourenkov, G. P., Bartunik, H. D., and Boos, W. (2000) X-ray structure of MalY from *Escherichia coli*: A pyridoxal 5′-phosphate-dependent enzyme acting as a modulator in mal gene expression, *EMBO J. 19*, 831−42.
31. Krissinel, E., and Henrick, K. (2004) Secondary-structure matching (SSM), a new tool for fast protein structure alignment in three dimensions, *Acta Crystallogr. D60*, 2256−68.
32. Anderson, J. W., Adediran, S. A., Charlier, P., Nguyen-Disteche, M., Frere, J. M., Nicholas, R. A., and Pratt, R. F. (2003) On the substrate specificity of bacterial DD-peptidases: Evidence from two series of peptidoglycan-mimetic peptides, *Biochem. J. 373*, 949−55.
33. Swaren, P., Golemi, D., Cabantous, S., Bulychev, A., Maveyraud, L., Mobashery, S., and Samama, J. P. (1999) X-ray structure of the Asn276Asp variant of the *Escherichia coli* TEM-1 β-lactamase: Direct observation of electrostatic modulation in resistance to inactivation by clavulanic acid, *Biochemistry 38*, 9570−6.
34. Gherman, B. F., Goldberg, S. D., Cornish, V. W., and Friesner, R. A. (2004) Mixed quantum mechanical/molecular mechanical (QM/MM) study of the deacylation reaction in a penicillin binding protein (PBP) versus in a class C β-lactamase, *J. Am. Chem. Soc. 126*, 7652−64.
35. Nicola, G., Peddi, S., Stefanova, M., Nicholas, R. A., Gutheil, W. G., and Davies, C. (2005) Crystal structure of *Escherichia coli* penicillin-binding protein 5 bound to a tripeptide boronic acid inhibitor: A role for Ser-110 in deacylation, *Biochemistry 44*, 8207−17.
36. Ishiguro, M., Nishihara, T., and Tanaka, R. (2001) New orally active penem antibiotic: Farom, *Yakugaku Zasshi 121*, 915−27.
37. Jelsch, C., Mourey, L., Masson, J. M., and Samama, J. P. (1993) Crystal structure of *Escherichia coli* TEM1 β-lactamase at 1.8 Å resolution, *Proteins 16*, 364−83.
38. Swaren, P., Maveyraud, L., Guillet, V., Masson, J. M., Mourey, L., and Samama, J. P. (1995) Electrostatic analysis of TEM1 β-lactamase: Effect of substrate binding, steep potential gradients and consequences of site-directed mutations, *Structure 3*, 603−13.
39. Maveyraud, L., Pratt, R. F., and Samama, J. P. (1998) Crystal structure of an acylation transition-state analog of the TEM-1 β-lactamase. Mechanistic implications for class A β-lactamases, *Biochemistry 37*, 2622−8.
40. Maveyraud, L., Saves, I., Burlet-Schiltz, O., Swaren, P., Masson, J. M., Delaire, M., Mourey, L., Prome, J. C., and Samama, J. P. (1996) Structural basis of extended spectrum TEM β-lactamases. Crystallographic, kinetic, and mass spectrometric investigations of enzyme mutants, *J. Biol. Chem. 271*, 10482−9.
41. Kraulis, P. J. (1991) MOLSCRIPT: A program to produce both detailed and schematic plots of protein structures, *J. Appl. Crystallogr. 24*, 946−50.
42. Merritt, E. A., and Bacon, D. J. (1997) Raster3D: Photorealistic Molecular Graphics, *Methods Enzymol. 277*, 505−24.

BI051533T